Oxidation of Alkyl Ions, $C_nH_{2n+1}^+$ ($n = 1-5$), in Reactions with O_2 and O_3 in the Gas Phase

Skip Williams,* W. B. Knighton,† Anthony J. Midey,‡ and A. A. Viggiano

Air Force Research Laboratory, Space Vehicles Directorate, 29 Randolph Road, Hanscom AFB, Massachusetts 01731-3010

Stephan Irle, Qingfang Wang, and Keiji Morokuma

Cherry L. Emerson Center for Scientific Computation and Chemistry Department, Emory University, 1515 Pierce Drive, Atlanta, Georgia 30322

Received: September 24, 2003

Rate constants and product ion branching fractions are reported for the reactions of CH_3^+, $C_2H_5^+$, *s*-$C_3H_7^+$, *s*-$C_4H_9^+$, *t*-$C_4H_9^+$, and *t*-$C_5H_{11}^+$ with O_2 and O_3 at 300 K in a variable-temperature selected-ion flow tube (VT-SIFT). The reaction rate constant for CH_3^+ with O_3 is large and approximately equal to the thermal energy capture rate constant given by the Su−Chesnavich equation. The $C_2H_5^+$, *s*-$C_3H_7^+$, and *s*-$C_4H_9^+$ ions are somewhat less reactive, reacting at approximately 7−46% of the thermal capture rate. The HCO^+ and $C_2H_3O^+$ ions are the major products in these reactions. The *t*-$C_4H_9^+$ and *t*-$C_5H_{11}^+$ ions are found to be unreactive, with rate constants $<5 \times 10^{-12}$ cm^3 s^{-1}, which is the present detection limit of our apparatus using this ozone source. Ozone is a singlet in its ground state, and ab initio calculations at the B3LYP/6-31G(d) level of theory indicate that reactant complexes can be formed, decreasing in stability with the size of alkyl chains attached to the cationic carbon atom. The decreasing reactivity of the alkyl ions with increasing order of the carbocation is attributed to a greatly reduced O_3 binding energy. The ions listed above do not undergo two-body reactions with O_2, $k < 5 \times 10^{-13}$ cm^3 s^{-1}, despite the availability of reaction channels with exothermicities of several hundred kilojoules per mole. Ab initio calculations at the B3LYP/6-31G(d) level of theory indicate that the O_2 reaction systems form weak complexes with large C−O bond distances (repulsive at smaller distances) on the lowest energy triplet potential energy surface. Access to the singlet surface is required for bond formation; however, this surface is not accessible at thermal energies.

I. Introduction

Carbonium ions are found in a wide variety of environments, including interstellar clouds, chemical vapor deposition plasmas, and combustion environments. Studies of the oxidation of these ions have historically been focused on $C_nH_m^+$ ion reactions with O atoms. These reactions have been studied to elucidate the synthetic chemistry occurring in interstellar clouds. Fehsenfeld[1] examined the reaction of CH_3^+, Bohme, Mackay, and Schiff[2] examined the reaction of CH_5^+, and Viggiano et al.[3,4] examined reactions of CH^+, CH_5^+, C_2^+, C_2H^+, and $C_2H_2^+$ and later isotopomers of CH_3^+ ($CD_nH_{3-n}^+$). More recently, Le Page et al.[5,6] reported the investigation of aromatic hydrocarbon ions $C_{10}H_6^+$, $C_{10}H_7^+$, and $C_{10}H_8^+$ and $C_{16}H_{10}^+$, $C_{16}H_9^+$, and $C_{16}H_{11}^+$ with H, N, and O atoms. Of these ions, $C_{10}H_8^+$, $C_{16}H_{10}^+$, and $C_{16}H_9^+$ were found to react with atomic oxygen. The $C_{16}H_9^+$ cation showed striking reactivity toward atoms, compared to the relative reactivity of phenylium and naphthylium ions, which was attributed to the triplet nature of the $C_{16}H_9^+$ ion in its ground state. Results of a study of 13 $C_mH_n^+$ ions ($m \leq 6$) with O, O_2, and NO carried out by Scott et al.[7] showed that most of the hydrocarbon ions studied exhibit relatively rapid reactions with O atoms that proceed at substantial fractions of the collision rate. One notable exception found by Scott et al. was the $C_2H_5^+$ ion, one of the subject ions in the present study, which showed no reactivity with O atoms.

The formation and destruction mechanisms of hydrocarbon ions in combustion environments is an area of recent interest. In particular, plasma sources are being explored as ignition and combustion aides in supersonic combustion, where fuel activation and initiation on fast-flow time scales pose a daunting challenge.[8] However, the information gained from these studies is broadly applicable to a wide range of problems such as spark inhibition, improved engine performance, service life, explosion limits in blended fuels, hydrocarbon molecular growth, and ignition. The oxidation of hydrocarbon ions in these environments is of fundamental interest. For example, $C_nH_m^+$, $C_nH_mO^+$, and $C_nH_mO_2^+$ positive ions have been observed in the flames of a variety of fuels.[9] Although these ions are commonly observed, their formation mechanisms are not fully understood.

One mechanism involves oxidation of hydrocarbon ions in a single step via reactions with oxygen species such as O, O_2, O_2 ($a\ ^1\Delta$), and O_3. As mentioned above, some work has been carried out with regard to O atom reactions, but the other oxidation processes remain relatively unexplored. The reactions of alkyl ions with numerous compounds have been reported previously.[10] However, reactions leading to the oxidation of $C_nH_{2n+1}^+$ ($n = 2-5$) species have not been reported. Oxidation of other organic ions with O_3 has been studied in the gas phase by Mendes et al.[11] using a pentaquadrupole mass spectrometer. The collision energy of the ion−molecule reactions studied in those experiments was ca. 1 eV. Mendes et al.[11] found that neutral ozone transfers an oxygen atom to several positive ions, namely, radical cations of pyridines, alkyl halides, and halogen cations. A

* Corresponding author.
† Permanent address: Department of Chemistry, Montana State University, Bozeman, MT.
‡ Under contract to Visidyne Inc., Burlington, MA, 01803.

10.1021/jp031099+ CCC: $27.50
Published on Web 02/20/2004

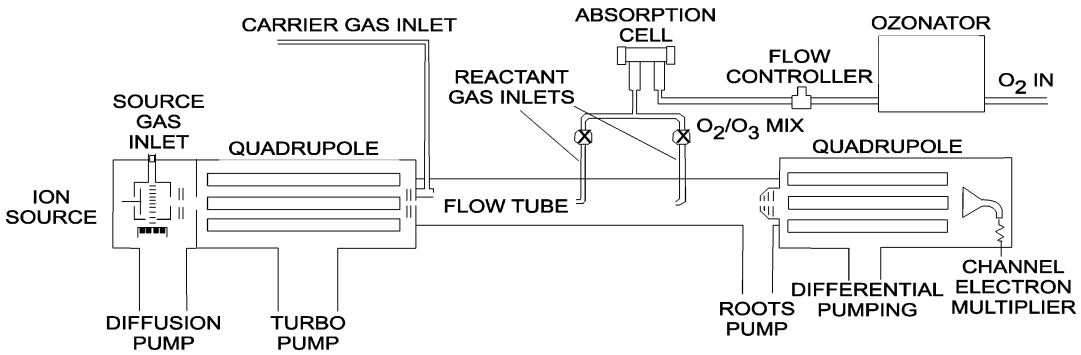

Figure 1. Overview of the selected-ion flow tube (SIFT) with ozonator and absorption cell.

considerable amount of O_2 was present in these experiments. However, when the experiments were repeated with pure O_2, no O-atom-transfer products were observed, confirming that the oxidation occurs from O_3 alone. Ab initio calculations were also performed as part of the work by Mendes et al.[11] to rationalize the formation of the reaction products observed. An interesting conclusion of that work is that simple nucleophilic addition of ozone followed by O_2 loss is the most likely mechanism for O-atom transfer from ozone to radical cations of pyridines, alkyl halides, and halogen cations. This new mechanistic pathway was suggested to be an important pathway for the generation of chemically interesting but difficult-to-generate ionized oxides.

In this paper, the chemistry of ionized hydrocarbons reacting with oxygen and ozone is investigated at 300 K using fast ion flow tube kinetics instrumentation. The measurements are conducted with a selected-ion flow tube (SIFT) instrument at ca. 0.5 Torr helium buffer pressure, and the kinetics are observed over ca. 3−4 ms reaction time. Specifically, rate constants and product ion branching fractions are reported for the reactions of CH_3^+, $C_2H_5^+$, *s*-$C_3H_7^+$, *s*-$C_4H_9^+$, *t*-$C_4H_9^+$, and *t*-$C_5H_{11}^+$ with O_2 and O_3 at room temperature. The HCO^+ ion is a major product in many of these reactions, so the reactivity of HCO^+ with O_2 and O_3 is also investigated. Density functional calculations using the B3LYP functional[12−14] and 6-31G(d) basis set[15] are also performed on the electronic ground-state potential surfaces of complexes of O_2 and O_3 with select hydrocarbon radical cations to elucidate the reaction mechanism leading to the oxidation of these ions. The new experimental findings are discussed in the context of these theoretical calculations and previous work where available.

II. Method

Experimental Details. The measurements were made at 300 K using the SIFT instrument at the Air Force Research Laboratory. This apparatus is described in detail elsewhere,[16,17] and the modifications required to perform experiments with ozone as a reactant gas have been discussed recently.[18] The SIFT is shown schematically, with modifications, in Figure 1.

In brief, carbonium ions are prepared in a remote, differentially pumped chamber by electron impact ionization of alkyl bromides and alkyl chlorides entrained within a supersonic argon expansion. After a skimmer, all ions are directed into a quadrupole mass filter, where the ionic species of interest is mass-selected. The mass-selected ions are injected via a Venturi-type inlet into a fast flow of helium carrier gas in a meter-long stainless steel flow tube. Reactant gas is introduced into the flow tube through either of two stainless steel reactant gas inlets and allowed to react over a known distance at a known flow velocity. The SIFT operates at ca. 0.5 Torr helium buffer pressure, and the kinetics are observed over ca. 3−4 ms reaction time. A second quadrupole mass spectrometer resolves the reactant and the product ions, which are then detected by an electron multiplier. Extrapolations of product branching fractions to zero reactant flow yield the nascent branching fraction. The decay in the primary reactant ion signal as a function of increasing reactant gas flow rate yields the reaction rate constant. Concentrations are such that [buffer] ≫ [reactant neutral] ≫ [ions]. Under these conditions, pseudo-first-order kinetics apply, and the rate constant is given by

$$k = \frac{1}{[\mathrm{B}]\tau} \ln \frac{[\mathrm{A_o}^{\pm}]}{[\mathrm{A}^{\pm}]} \qquad (1)$$

where k is the rate constant, τ is the reaction time, [B] is reactant neutral concentration, and $[A_o^{\pm}]$ and $[A^{\pm}]$ are the primary reactant ion concentrations in the absence and in the presence of reactant neutral, respectively. The reaction time, τ, is the reaction distance divided by the buffer velocity multiplied by a correction factor determined from previous time-of-flight measurements that accounts for the fact that both the ion velocity and the ion concentration are at a maximum along the axis of the flow tube. A typical value for the correction factor is 1.6. The buffer velocity is obtained from the mass flow rate of the buffer, the flow tube cross section, temperature, and pressure in the normal manner.[19] The absolute uncertainties of the rate constants are 25%, and relative uncertainties are 15%.

An Orec O3V-0 ozonator was interfaced to the SIFT apparatus to produce the ozone reactant gas used in this experiment. A commercial supply of O_2 (Airco, 99.999%) was used to manufacture the ozone. The O_3 was produced at a pressure of 3−6 psig using a 0.9-A discharge current. The resulting reactant gas is approximately 5% O_3 in O_2, which is the same as that reported previously by Fahey et al.[20] The fraction of O_3 was relatively independent of the reactant gas flow rate over a 100 SCCM flow range. The presence of O_2 does not affect the measurements, because O_2 was found to be unreactive with the positive ions studied here, including the product ions. Flow contamination was less than 0.05%, typically arising from nitrogen and carbon dioxide trace gases in the ozonator and the tubing. Flushing the lines and the ozonator regularly to prevent the buildup of NO_2, NO_3, and CO_2 minimized contamination. All fittings and valves used in the O_3 delivery system are stainless steel, and the tubing was either stainless steel or Teflon.

A flow controller regulates the O_3/O_2 reactant mixture flow into a 10.2-cm-long, 1.3-cm-diameter Pyrex absorption cell fitted with quartz windows. The absorption cell is connected to the flow tube stainless steel reactant inlets by approximately 40 cm of 0.25-in.-o.d. Teflon tubing. Varying the length of the Teflon tubing from 40 to 300 cm produced no difference (<5%) in

the results, suggesting that no significant O_3 decomposition occurs in the tubing. The absolute concentration of O_3 is measured by optical absorption at 248 and 254 nm using a Perkin-Elmer Lambda 10 UV/vis spectrometer. The concentration of the ozone in the flow tube was found using

$$[O_3] = \left(\frac{2.303A}{\sigma_\lambda\, l}\right)\left(\frac{P_{FT}}{P_{AC}}\right)\left(\frac{F_{AC}}{F_{FT}}\right) \qquad (2)$$

where A is the log absorbance (base 10) output from the spectrometer, σ_λ (cm^2 $molecule^{-1}$) is the absorption cross section for O_3 at wavelength λ, l is the length of the absorption cell in cm, P_{FT} is the flow tube pressure, P_{AC} is the absorption cell pressure, F_{AC} is the total flow through the absorption cell, and F_{FT} is the total flow through the flow tube. The 248- and 254-nm cross sections used were 1.08×10^{-17} and 1.137×10^{-17} cm^2 $molecule^{-1}$, respectively.[21,22] In our previous publication,[18] results regarding several negative-ion reactions with ozone were compared to literature values regarding the negative-ion chemistry of ozone, which prior to our study lacked sufficient agreement for application to detailed physical models. For the reaction of SF_6^- with ozone, there is now good agreement between three recent measurements,[18] indicating reliable delivery and knowledge of the O_3 concentrations in the present experiment.

CH_3^+ was prepared by ionizing methyl bromide (Aldrich, >99.5%), $C_2H_5^+$ was prepared by ionizing ethyl bromide (Aldrich, >99%), $C_3H_7^+$ was prepared by ionizing isopropyl bromide (Aldrich, >99%), *n*-$C_3H_7^+$ was prepared by ionizing *n*-propyl bromide (Aldrich, >99%), *t*-$C_4H_9^+$ was prepared by ionizing *tert*-butyl chloride (Aldrich, >99%), *s*-$C_4H_9^+$ was prepared by ionizing *n*-butyl chloride (Aldrich, >99%), and $C_5H_{11}^+$ was prepared by ionizing 2-chloro-2-methylbutane. HCO^+ was formed by ionizing CO (Airco, 99.9%) in the supersonic source and injecting CO^+ into the flow tube, which is reacted with 10 SCCM of H_2 added 20 cm upstream of the reactant inlet. All source gases were entrained within a supersonic argon (Airco, 99.995%) expansion.

Calculations. Geometry optimizations were carried out using Gaussian's implementation of the B3LYP hybrid density functional[12−14] using the standard 6-31G(d) basis set of Pople et al.[15] Open-shell fragments were treated using the spin-unrestricted density funcional formalism. Analytical frequency calculations were used to characterize the nature of these stationary points. All of the reaction pathways were verified by intrinsic reaction coordinate (IRC) calculations[23−27] both forward and backward from the encountered transition states. Standard Mulliken population analysis[28−30] was employed to analyze electron density and spin density distributions from the B3LYP/6-31G(d) densities.

III. Results

Reaction rate constants and product branching fractions for alkyl ions, $C_nH_{2n+1}^+$ ($n = 1-5$), and HCO^+ reacting with O_3 measured at 300 K with the SIFT are shown in Table 1. None of the subject cations showed any measurable bimolecular reactivity with O_2, $k < 5 \times 10^{-13}$ cm^3 s^{-1}. In Table 1, the standard reaction enthalpies at 298 K (in kJ mol^{-1}) have been calculated and are listed. The heats of formation are taken from the NIST compilation.[31,32] Note that the *tert*-butyl ion heat of formation has been recently revised, and a value of $\Delta H_f^\circ{}_{298}$(*t*-$C_4H_9^+$) = 711 kJ/mol from recent experimental[33−35] and theoretical studies[36] is used, which is 20 kJ/mol higher than previous experimental measurements. Figure 2 shows corrected

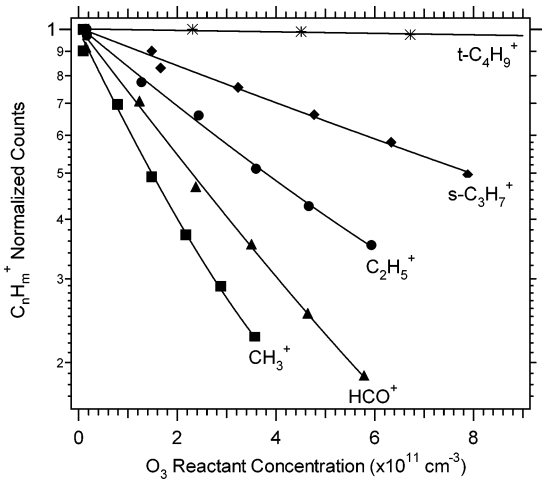

Figure 2. Corrected (see text) primary ion decay plots for CH_3^+ (■), HCO^+ (▲), $C_2H_5^+$ (●), *s*-$C_3H_7^+$ (◆), and *t*-$C_4H_9^+$ (∗) reacting with O_3. The solid lines are nonlinear least-squares fits to the data, performed to determine the rate constants according to eq 1. Experiments are performed with a reactant gas composition of 5% O_3 in O_2, which is possible since O_2 is unreactive.

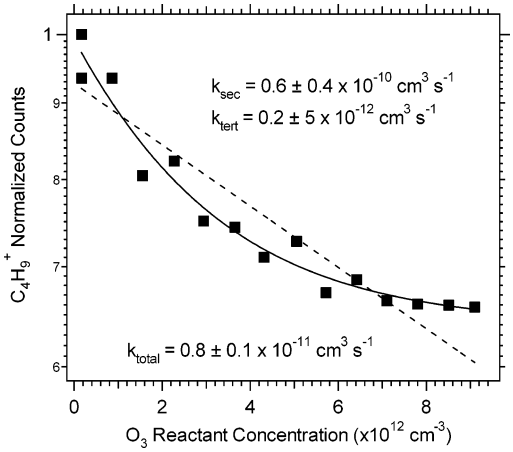

Figure 3. Normalized $C_4H_9^+$ counts (■) plotted vs O_3 concentration. The dashed line is the result of a single-exponential fit of the data to determine the rate constant according to eq 1. The result of the single-exponential fit is labeled k_{total}. The solid line is the result of a double-exponential fit of the data which yields a fast component (k_{sec}) with a rate constant of $(6 \pm 4) \times 10^{-11}$ cm^3 s^{-1} and a slow component (k_{tert}) with a rate constant $<5 \times 10^{-12}$ cm^3 s^{-1}.

(see below) primary ion decay plots for the reactions of CH_3^+, HCO^+, $C_2H_5^+$, *s*-$C_3H_7^+$, and *t*-$C_4H_9^+$ with O_3. The solid lines are linear least-squares fits to the data, performed to determine the rate constants according to eq 1. Sample kinetics data for $C_4H_9^+$, prepared by ionizing *n*-butyl bromide, are shown in Figure 3. Electron impact ionization of *n*-butyl bromide is expected to produce both *s*-$C_4H_9^+$ and *t*-$C_4H_9^+$.[37] The isomeric composition was determined by exploiting the order of magnitude difference in the hydride-transfer reaction rate constant with 2-methylpentane (*i*-C_5H_{12}) for the two isomers, as shown in Figure 4. The specific results for each cation studied are discussed below.

HCO^+ Cation. The HCO^+ cation is a major product of the primary and secondary carbocation reactions with O_3 listed in Table 1. Hence, the reactivity of HCO^+ with O_3 was included in this study. In these studies, CO^+ was injected into the flow tube and reacted with 10 SCCM of H_2 added at inlet 1. This provided a source of HCO^+, although other ions including H_3O^+ and O_2^+ were present in trace amounts. The SIFT spectrum of CO^+ in the absence of added H_2 indicated the presence of H_2O^+

TABLE 1: Reaction Rate Constants for Reactions of Ozone at 300 K, Measured with the Selected-Ion Flow Tube (SIFT)

reaction	products	k, [k_c] ($\times 10^{-9}$ cm^3 s^{-1})	branching fractions	ΔH (kJ/mol)
$HCO^+ + O_3 \rightarrow$		*1.2, [1.3]*		
	$HO_3^+ + CO$		>0.98	−31.5
$CH_3^+ + O_3 \rightarrow$		*1.7, [1.6]*		
	$HCO^+ + (H_2 + O_2)$		0.66	−410
	$H_2CO^+ + HO_2$		0.16	−293
	$H_2O_2^+ + HCO$		0.10	−311
	$O_2^+ + CH_3O$		0.07	−54
	$H_3O^+ + CO_2$		<0.01	−1038
$C_2H_5^+ + O_3 \rightarrow$		*0.59, [1.3]*		
	$HCO^+ + (CH_4 + O_2)$		0.70	−294
	$C_2H_3O^+ + (H_2 + O_2)$		0.30	−392
s-$C_3H_7^+ + O_3 \rightarrow$		*0.22, [1.2]*		
	$C_2H_3O^+ + (CH_4 + O_2)$		0.64	−363
	$HCO^+ + (C_2H_6 + O_2)$		0.16	−200
	$CH_3O^+ + C_2H_4 + O_2$		0.14	−186
	$CH_3O^+ + CH_3COOH$			−670
	$C_3H_3O^+ + 2H_2O$		0.05	−674
	$C_3H_6O^+ + HO_2$		0.01	−167
s-$C_4H_9^+ + O_3 \rightarrow$		*0.08, [1.1]*		
	$HCO^+ + (C_3H_8 + O_2)$		major (∼0.40)	−188
	$C_2H_3O^+ + (C_2H_6 + O_2)$		major (∼0.35)	−339
	$C_2H_5O^+ + C_2H_4 + O_2$		minor (∼0.14)	−273
	$C_2H_5O^+ + CH_3COOH$			−758
	$C_2H_2O^+ + C_2H_6 + HO_2$		minor (∼0.09)	−111
	$CH_3O^+, C_3H_3O^+, C_3H_5O^+$		trace (<0.02)	
t-$C_4H_9^+ + O_3 \rightarrow$		*<0.005, [1.1]*		
	$C_2H_3O^+ + (C_2H_6 + O_2)$			−284
	$HCO^+ + (C_3H_8 + O_2)$			−133
t-$C_5H_{11}^+ + O_3 \rightarrow$		*<0.005, [1.1]*		
	$C_2H_5CO^+ + (C_2H_6 + O_2)$			−296
	$C_2H_3O^+ + (C_3H_8 + O_2)$			−255
	$HCO^+ + (C_4H_{10} + O_2)$			−112

[a] All of the cations listed showed no reactivity, $k < 5 \times 10^{-13}$ cm^3 s^{-1}, with O_2. The calculated collision rate constant, k_c, and the measured rate constant, k, are listed in italics. The reaction products and branching fractions are listed under the rate constants. Energetics are taken from the NIST Chemistry WebBook.[31,32] Neutral products are not resolved in these experiments. Brackets indicate that more than one product channel could contribute to the branching fraction. Products contained in parentheses are estimated on the basis of the mechanism discussed in the text involving O_2 loss. Note that the reactions are considerably more exothermic if the reaction products in parentheses are not dissociated.

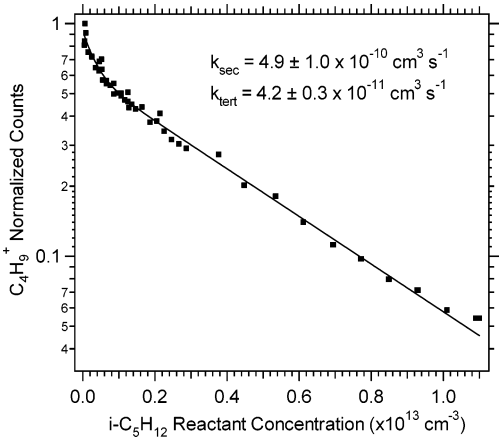

Figure 4. Normalized $C_4H_9^+$ counts (■) plotted vs 2-methylpentane (*i*-C_5H_{12}) concentration. The solid line is the result of a double-exponential fit of the data which yields a fast component (k_{sec}) with a rate constant of $(4.9 \pm 1.0) \times 10^{-10}$ cm^3 s^{-1} and a slow component (k_{tert}) with a rate constant $(4.2 \pm 0.3) \times 10^{-11}$ cm^3 s^{-1}.

and O_2^+, which indicates that the source chemistry is responsible for the background levels of H_3O^+ and O_2^+. HCO^+ is known to be unreactive with O_2,[38] and that finding was confirmed in this study. However, HCO^+ is very reactive with O_3, which is expected since the isoelectronic hydrogen cyanide molecule is known to react with ozone to produce HCNO as a major product.[39] The major product of HCO^+ reacting with O_3 is HO_3^+. The branching fraction reported in Table 1 is >0.98 and is intended to reflect the uncertainty of the source conditions. The measured rate constant of 1.2×10^{-9} cm^3 s^{-1} is nearly equal to the thermal capture rate constant of 1.3×10^{-9} cm^3 s^{-1}.

Methyl Cation. The methyl cation was prepared by ionization of methyl bromide and was selectively injected into the flow tube. However, despite very low injection energies, approximately 12% of the CH_3^+ collisionally dissociated to form CH^+ and CH_2^+. While these breakup products do not interfere with the reaction rate constant determination, they do react with O_2 to form some of the same products observed in the $CH_3^+ + O_3$ reaction.[40] Namely, CH^+ and CH_2^+ react with O_2 with rate constants of 9.7×10^{-10} and 9.1×10^{-10} cm^3 s^{-1}, respectively, and produce the following products:[40]

$$CH^+ + O_2 \rightarrow HCO^+ + O \quad \text{(major)} \quad (3a)$$

$$\rightarrow O^+ + HCO \quad \text{(minor)} \quad (3b)$$

$$\rightarrow CO^+ + OH \quad \text{(minor)} \quad (3c)$$

and

$$CH_2^+ + O_2 \rightarrow HCO^+ + OH \quad \text{(major)} \quad (4a)$$

$$\rightarrow H_2CO^+ + O \quad \text{(minor)} \quad (4b)$$

The methyl cation, on the other hand, does not undergo two-

body reactions with O_2 and only exhibits a slow ternary association reaction, $k_{300\,K} = 8.6 \times 10^{-30}$ cm^6 s^{-1}.[40,41]

Therefore, the impurity CH^+ and CH_2^+ ions were eliminated before entering the reaction zone by addition of a small amount (5 SCCM) of O_2 approximately 20 cm upstream of the first reactant inlet. The O^+ and CO^+ ions resulting from reactions 3b and 3c are converted to O_2^+ via charge transfer with O_2, and the H_2CO^+ from reaction 4b is converted to HCO^+ (major) and $H_2O_2^+$ (minor) via reaction with O_2. After the addition of O_2 at inlet 1, the resulting ion composition in the flow tube at the reactant inlet was observed to be approximately 88% CH_3^+, 8.5% HCO^+, 2.5% O_2^+, and ~1% $H_2O_2^+$. The O_2^+ and $H_2O_2^+$ ions were accounted for by subtracting their baseline intensities observed at zero O_2/O_3 reactant flow from the appropriate product ion intensities. The HCO^+ ion counts observed at zero O_2/O_3 reactant flow were corrected for by subtracting the appropriate number of counts at each ozone concentration, on the basis of the reactivity of HCO^+ with O_3 listed in Table 1.

The methyl cation reacts at the collision rate with O_3, producing HCO^+ as a major product and H_2CO^+, $H_2O_2^+$, O_2^+, and H_3O^+ as minor products. The product ion counts observed for H_2CO^+, $H_2O_2^+$, and O_2^+ were significantly above the background counts discussed for these ions. Therefore, these ions are confirmed products. The H_3O^+ product, on the other hand, results either from direct reaction of CH_3^+ with O_3, which is highly exothermic but involves significant rearrangement, or from secondary reactions of HCO^+ with the very low level of H_2O present in the flow tube. Secondary chemistry can be accounted for by extrapolating the baseline-corrected product branching fraction back to zero reactant concentration.[18] However, this approach did not fully account for the amount of H_3O^+ observed. Therefore, H_3O^+ is listed as a trace product in the reaction of $CH_3^+ + O_3$.

Ethyl Cation. The ethyl cation, prepared by ionizing ethyl bromide, reacts with O_3 to form two primary products, HCO^+ and $C_2H_3O^+$. Because $C_2H_5^+$ and HCO^+ are mass-coincident, two separate experiments were performed to determine the reaction rate constant. One experiment involved the addition of CH_3Cl to the flow tube via inlet 1. Methyl chloride reacts with HCO^+ by proton transfer to form CH_4Cl^+ and was not intended to react with $C_2H_5^+$. However, the addition of methyl chloride did cause a reduction in the $C_2H_5^+$ signal and produced several unidentified high-mass ions containing chlorine, so the amount of methyl chloride added was such that only about 20% of the original $C_2H_5^+$ signal remained. In a second experiment, $^{13}CCH_5^+$ ion was injected into the flow tube. Statistically equal amounts of $^{12}CHO^+$ and $^{13}CHO^+$ are assumed to be formed, and the intensity of $^{12}CHO^+$ is used as a measure of the $^{13}CHO^+$ contribution to the $m/z = 30$ (sum of $^{13}CCH_5^+ + {}^{13}CHO^+$). The reaction rate constant was determined by subtracting the intensity monitored at m/z 29 ($^{12}CHO^+$) from that at $m/z = 30$ (sum of $^{13}CCH_5^+ + {}^{13}CHO^+$) and plotting the decay of the resulting ion signal as a function of O_3 flow. The two different experiments produced the following results. Using the methyl chloride scavenger, three determinations yielded rate constants of 6.3×10^{-10}, 6.5×10^{-10}, and 5.7×10^{-10} cm^3 s^{-1}. The $^{13}CCH_5^+$ experiment in a single determination yielded 5.2×10^{-10} cm^3 s^{-1}. The reaction rate constant in Table 1 is the average of the four measurements.

The reaction product branching fraction was estimated by reacting the ^{12}C form of $C_2H_5^+$ with high O_3 concentrations where no intensity at $m/z = 29$ remained, i.e., $C_2H_5^+$ totally reacted and all of the HCO^+ was converted to HO_3^+. Approximately 5% of the $C_2H_5^+$ dissociated to $C_2H_3^+$ upon injection into the flow tube. The reaction products originating from $C_2H_3^+$ were not identified or corrected for and constitute no more than a 5 percentage point uncertainty, i.e., the original fraction of the $C_2H_3^+$ reactant ion intensity, assuming it yields only a single product in the reported values. Since there are no minor channels, the presence of $C_2H_3^+$ has a small effect on the overall reported branching fractions.

***sec*-Propyl Cation.** The propyl radical cation was prepared by ionizing isopropyl bromide in the supersonic source. Approximately 5% of the $C_3H_7^+$ dissociated to $C_3H_5^+$ upon injection into the flow tube. Because $C_2H_3O^+$ is a major product of the *sec*-propyl cation reaction with O_3 and is mass-coincident with $C_3H_7^+$, the reaction rate constant was determined by injecting the $^{13}CC_2H_7^+$ ($m/z = 44$) form of the reactant ion. Given that the expected $C_2H_3O^+$ product distribution is 33% $C_2H_3O^+$ ($m/z = 43$) and 67% $^{13}CCH_3O^+$ ($m/z = 44$), then the $I(^{13}CC_2H_7^+) = I(m/z = 44) - 2I(m/z = 43)$. The reaction rate constant was determined using this corrected $C_3H_7^+$ intensity. The product branching fractions were determined from the same ^{13}C experiments as follows: $I(C_2H_3O^+) = 3I(^{12}C_2H_3O^+)$, $I(HCO^+) = I(^{12}CHO^+) + I(^{13}CHO^+)$, and $I(CH_3O^+) = I(^{12}CH_3O^+) + I(^{13}CH_3O^+)$, with the remaining C_3 products exhibiting only a single peak. Three determinations were averaged and yielded 16% CHO^+, 14% CH_3O^+, 64% $C_2H_3O^+$, 5% $C_3H_3O^+$, and 1% $C_3H_6O^+$. The reaction products originating from $C_3H_5^+$ have not been positively identified but can be deduced to be either CHO^+ and/or $C_2H_3O^+$, on the basis of the observed product distributions for the $C_3H_7^+$ and *s*-$C_4H_9^+$ (see below) reactant ions. Note that both $C_3H_7^+$ and *s*-$C_4H_9^+$ show a small amount of dissociation to $C_3H_5^+$ upon injection into the flow tube and that only products common to both reaction systems can be possible reaction products of $C_3H_5^+$ and O_3. The influence of the $C_3H_5^+$ on the reported branching fractions has not been corrected for but constitutes no more than a 5 percentage point uncertainty (original fraction of the reactant ion intensity yielding a single product) in the reported values of the HCO^+ and $C_2H_3O^+$ product channels.

Previous theoretical studies at the Hartree−Fock and MP2 levels of theory on the character of the potential energy surface of the propyl cation[42] conclude that there exist two global minima, that for the *sec*-propyl cation and that for corner-protonated cyclopropane. These calculations showed that a minimum does not exist that corresponds to the *n*-propyl cation, which appears to be only a transition structure in the interconversion of the *sec*-propyl cation and the corner-protonated cyclopropane cation. According to these calculations, the *n*-propyl cation is 80.5 kJ/mol higher and the corner-protonated cyclopropane cation is 30 kJ/mol higher in energy than the *sec*-propyl cation structure. Our B3LYP/6-31G(d) calculations are consistent with these findings. Furthermore, experimental investigations of the interconversion of the propyl cation structures demonstrate rapid rearrangement to the *sec*-propyl cation form. A detailed study by Ausloos and co-workers[43] showed that *n*-propyl cations isomerize intramolecularly to either isopropyl ions or protonated cyclopropane ions within 10^{-10} s. Rearrangement to the isopropyl ion is favored and increases in importance with increasing internal energy content of the ion. Mass spectrometric investigations suggest that the isomerization of the corner-protonated cyclopropane structure to the isopropyl structure requires 10^{-7}−10^{-5} s.[44,45] All of these isomerization times are much shorter than the approximately 1 ms it takes the ions to leave the source region and travel to the reactant inlet. Therefore, the reactivity shown in Table 1 for the propyl cation has been assigned to the *s*-$C_3H_7^+$ isomer.

To confirm this hypothesis, the propyl cation was also prepared by ionizing *n*-propyl bromide in the supersonic source. The kinetics measurements were performed using the $^{13}CC_2H_7^+$ ion and corrected for $^{13}CCH_3O^+$ product as described in the experimental details using isopropyl bromide in the source. The product branching distribution was determined from the mass spectrum recorded with 100 SCCM of O_3, where no $C_3H_7^+$ remains. As above, no correction for the products originating from $C_3H_5^+$ (~5% of the original reactant ion intensity) was made. The reaction rate constants and the product distributions for the $C_3H_7^+$ ions generated from *n*-propyl bromide are found to be nearly identical to those produced from isopropyl bromide. The minor differences observed in the branching ratios can be attributed to statistical deviations in the reproducibility of the measurements and small differences in the source and injection conditions. This result is consistent with the theoretical and experimental studies discussed above regarding the stability and isomerization processes of the $C_3H_7^+$ ions, which indicate that only the *s*-$C_3H_7^+$ isomeric form of the ion is present in our experiments.

***tert*-Butyl Cation.** In pulsed ion cyclotron resonance (ICR) experiments, Shold and Ausloos[37] observed that $C_4H_9^+$ cations formed by electron impact ionization of isobutane, neopentane, 2,2-dimethylbutane, isobutyl halides, and *tert*-butyl halides all have the tertiary structure. Fragmentation of *n*-alkanes, 2-methylbutane, 3-methylpentane, *n*-butyl halides, and *sec*-butyl halides produce both *s*-$C_4H_9^+$ and *t*-$C_4H_9^+$, with the *s*-$C_4H_9^+$ surviving without rearrangement for at least 0.1 s. However, in the case of the halides, a collision-induced isomerization of the *s*-$C_4H_9^+$ to the *t*-$C_4H_9^+$ was found to occur. The ICR experiments of Shold and Ausloos were conducted at pressures of ca. 10^{-6} Torr and observation times ranging from 10^{-3} to 0.5 s. The temperature in the analyzer cell was kept at 320 K, and the electron energy was varied between 10 and 25 eV.[37]

On the basis of the Shold Ausloos results,[37] the *tert*-butyl cation was prepared by electron impact ionization of *tert*-butyl chloride in the supersonic argon expansion. The reported reaction rate constant was measured by increasing the flow tube pressure to 0.64 Torr (throttling the roots pump) and provided a measured value of $<3.4 \times 10^{-12}$ cm^3 s^{-1}, which is at the detection limit of our experiments and therefore represents an upper limit. No reactivity of *t*-$C_4H_9^+$ with O_2 was observed either, i.e., $k < 3 \times 10^{-13}$ cm^3 s^{-1}.

***sec*-Butyl Cation.** The *sec*-butyl cation was prepared by ionizing *n*-butyl bromide in the supersonic source. Injection of $C_4H_9^+$ into the flow tube yielded approximately 93% $C_4H_9^+$, 5% $C_3H_5^+$, and 2% $C_2H_5^+$. The electron impact ionization of *n*-butyl bromide produces both *s*-$C_4H_9^+$ and *t*-$C_4H_9^+$, and collisions with halide molecules in the source region can convert *s*-$C_4H_9^+$ to *t*-$C_4H_9^+$.[37] The kinetics plots with the $C_4H_9^+$ cation exhibited curvature indicating the presence of more than one form of $C_4H_9^+$. Using a large number of flow points and fitting the data as a double exponential with a nonlinear least-squares analysis program provides an estimate of the relative amounts of the two types of $C_4H_9^+$ and a measure of the rate constant for the fast-reacting species. Figure 3 shows the normalized counts of the $C_4H_9^+$ reactant ion plotted as a function of the ozone reactant concentration. The result of a single-exponential fit to the data yielded the dashed line associated with the rate constant designated k_{total}. The single-exponential fit reproduces the data very poorly. However, a double-exponential fit provides a much better representation of the data. Free fitting several sets of data for the two rate constants yields a fast component with a rate constant of 8×10^{-11} cm^3 s^{-1} and a slow component with a rate constant $<4 \times 10^{-12}$ cm^3 s^{-1}. No reactivity of either form of $C_4H_9^+$ with O_2 was observed, i.e., $k < 3 \times 10^{-13}$ cm^3 s^{-1}, which is the detection limit of the experiment. It is assumed that the slower reacting component is the *tert*-butyl cation (ca. 67%) and the faster reacting component is *sec*-butyl cation (ca. 33%).

Additional insight into the relative amounts of the different forms of $C_4H_9^+$ was explored using 2-methylbutane as the neutral reactant in hydride-transfer reactions, as done by Shold and Ausloos[37] and Meot-Ner and Field.[46] The tertiary and secondary forms of $C_4H_9^+$ have markedly different rates for hydride transfer from 2-methylbutane (*i*-C_5H_{12}). On the basis of previous results,[10,46] the hydride-transfer rate constants for the reactions

$$t\text{-}C_4H_9^+ + (CH_3)_2CHCH_2CH_3 \rightarrow i\text{-}C_4H_{10} + t\text{-}C_5H_{11}^+, \quad k_{298\,K} = 2 \times 10^{-11}\ \text{cm}^3\ \text{s}^{-1} \quad (5a)$$

and

$$s\text{-}C_4H_9^+ + (CH_3)_2CHCH_2CH_3 \rightarrow n\text{-}C_4H_{10} + t\text{-}C_5H_{11}^+, \quad k_{298\,K} = 4 \times 10^{-10}\ \text{cm}^3\ \text{s}^{-1} \quad (5b)$$

differ by over an order of magnitude. Figure 4 shows a plot of the total $C_4H_9^+$ reaction ion concentration as a function of 2-methylbutane reactant concentration. A biexponential fit of the data plotted in Figure 4 yields two rate constants of $(4.9 \pm 1.9) \times 10^{-10}$ (35%) and $(4.2 \pm 1.4) \times 10^{-11}$ cm^3 s^{-1} (65%). These hydride-transfer rate constants are in good agreement with those reported previously, and this experiment confirms that approximately 35% of the ions formed under our conditions are *s*-$C_4H_9^+$.

The product branching measurements are considerably more difficult than those of the reaction rate constant because most of the $C_4H_9^+$ is the nonreactive tertiary form. Hence, the contributions of contaminant ions produced on breakup during injection, $C_2H_5^+$ and $C_3H_5^+$, are considerably larger compared to the products of the *s*-$C_4H_9^+$ primary ion. The major products observed are HCO^+ and $C_2H_3O^+$, and $C_2H_5O^+$ and $C_2H_2O^+$ are minor products. As shown in Table 1, the reaction of $C_2H_5^+$ with O_3 produces HCO^+ and $C_2H_3O^+$, and $C_2H_5^+$ is unreactive with O_2. Since $C_2H_2O^+$ and $C_2H_5O^+$ were not observed in the experiments discussed above that contain the $C_3H_5^+$ impurity ion, these products most likely originate from the reaction of *s*-$C_4H_9^+$ with O_3. Given this level of uncertainty, the only conclusions that can be drawn are that HCO^+ and $C_2H_3O^+$ are major products and that $C_2H_2O^+$ and $C_2H_5O^+$ are minor products produced in the reaction of *s*-$C_4H_9^+$ with O_3.

The production of $C_3H_5O^+$ in the reaction of *s*-$C_4H_9^+$ with O_3 is exothermic and is a conceivable product channel. The reaction for such a process is given below:

$$s\text{-}C_4H_9^+ + O_3 \rightarrow C_3H_5O^+ + CH_4 + O_2, \quad \Delta H = -393\ \text{kJ/mol} \quad (6)$$

Since $C_3H_5O^+$ is mass-coincident with $C_4H_9^+$, the $^{13}CC_3H_9^+$ ($m/z = 58$) form of the reactant ion was injected into the flow tube. Assuming a statistical ^{13}C product distribution, approximately 25% of the $C_3H_5O^+$ product ion produced should be $C_3H_5O^+$ ($m/z = 57$). Product branching fraction measurements taken at high resolution resulted in barely detectable amounts of $C_3H_3O^+$ ($m/z = 55$), $^{13}C_3H_3O^+$ ($m/z = 56$), and $C_3H_5O^+$ ($m/z = 57$) produced in the reaction. Trace amounts of ions at $m/z = 31$ and $m/z = 32$ were also observed and have

been assigned to CH_3O^+ ($m/z = 31$) and $^{13}CH_3O^+$ ($m/z = 32$). Note that the CH_3O^+, $C_3H_3O^+$, and $C_3H_5O^+$ product ions could also originate from reaction of the $C_3H_5^+$ breakup ion (5%) reacting with O_3. Therefore, the CH_3O^+, $C_3H_3O^+$, and $C_3H_5O^+$ product ions are listed as trace product ions in Table 1.

C_5H_{11} Cation. The $C_5H_{11}^+$ radical cation was prepared by ionizing 2-chloro-2-methylbutane. The reported reaction rate constant for the $C_5H_{11}^+$ ion formed after reaction with O_2 is $<3 \times 10^{-13}$ cm^3 s^{-1} and with O_3 is $<4 \times 10^{-12}$ cm^3 s^{-1}. The tertiary form of the $C_5H_{11}^+$ cation is the most stable form of this carbocation, and electron impact ionization of the 2-chloro-2-methylbutane ion precursor is expected to produce this ion exclusively. The *t*-$C_5H_{11}^+$ cation is the most stable cation studied in this series,[47] and, like the exceptionally stable *t*-$C_4H_9^+$ cation, it is not oxidized by either O_2 or O_3, even though several very exothermic products are available.

IV. Discussion

Cacace and co-workers first experimentally detected the elusive protonated ozone molecule, HO_3^+, in 1994 by reacting ozone with CH_5^+.[48] The present study shows that protonated ozone is produced efficiently by the reaction of HCO^+ with O_3 via a fast proton-transfer reaction, as listed in Table 1. The high efficiency is expected because the reaction is exothermic and spin-allowed, with singlet reactants producing singlet products. There are several other examples of efficient exothermic proton-transfer reactions in the literature[10] which have been discussed in detail.

In the early stages of combustion, O_2 is in large abundance, and even limited reactivity of hydrocarbon ions with O_2 could prove to be an important mechanism in these environments. However, none of the $C_nH_{2n+1}^+$ ($n = 1-5$) alkyl ions exhibited any appreciable reactivity with O_2. All of these cations are closed-shell singlet molecules, and O_2 is triplet in its ground state. The production of the OH radical is spin-allowed and is exothermic by over 90 kJ/mol for the $C_nH_{2n+1}^+$ ($n = 1-4$) alkyl ions. For example,

$$s\text{-}C_3H_7^+(^1A) + O_2(^3\Sigma) \rightarrow CH_2C(OH)CH_3^+(^2A'') + OH(^2\Pi) \quad (7)$$

is spin-allowed and exothermic by 99 kJ. The reaction products listed in reaction 7 require significant rearrangement, possibly though a strongly attractive intermediate complex. Several other exothermic reaction channels, requiring less rearrangement, are available but are spin-forbidden, namely,

$$s\text{-}C_3H_7^+ + O_2 \rightarrow CH_3O^+ + C_2H_4O, \quad \Delta H = -267 \text{ kJ/mol} \quad (8a)$$

$$\rightarrow C_2H_3O^+ + CH_3OH, \quad \Delta H = -249 \text{ kJ/mol} \quad (8b)$$

$$\rightarrow HCO^+ + C_2H_6O, \quad \Delta H = -209 \text{ kJ/mol} \quad (8c)$$

It is not necessary that a reaction proceed in a manner that allows for spin conservation. There are several ion−molecule reactions that have been observed to be fast despite violating spin conservation. Examples include

$$O^+(^4S) + CO_2(^1\Sigma) \rightarrow O_2^+(^2\Pi) + CO(^1\Sigma) \quad (9)$$

which proceeds at the collision rate,[49,50] the reaction of CH_3^+ with oxygen atoms,[1,4,7]

$$CH_3^+(^1A) + O(^3P) \rightarrow HCO^+(^1A) + H_2(^1\Sigma) \quad (10)$$

with a measured rate constant of 4.4×10^{-10} cm^3 s^{-1}, a number of positive-ion charge-transfer reactions where the rate constant exceeds the spin-conserving weighted collision rate constant,[51] as well as a number of hydrocarbon ion reactions with $N(^4S)$ atoms.[52]

Ab initio calculations regarding $C_2H_5^+$ and *s*-$C_3H_7^+$ reacting with O_2 at the B3LYP/6-31G(d) level of theory set suggest that these alkyl ions yield relatively weak complexes with O_2 with elongated C−O bond distances, namely,

$$C_2H_5^+(^1A) + O_2(^3\Sigma) \rightarrow [OOC_2H_5]^+*(^3A''), \quad \Delta H = -24 \text{ kJ/mol} \quad (11)$$

and

$$s\text{-}C_3H_7^+(^1A) + O_2(^3\Sigma) \rightarrow [OOCH(CH_3)CH_3]^+*(^3A''), \quad \Delta H = -13 \text{ kJ/mol} \quad (12)$$

The minimum calculated C−O bond distance for these complexes is ca. 2.6 Å with further C−O approach being repulsive, independent of the orientation of O_2 relative to the cation. These calculations suggest that no C−O bond can be formed on the triplet surface in these complexes, and that the singlet state required for bond formation is about 109 kJ/mol higher in energy. In addition, hydrogen atom and proton abstraction, which are spin-allowed, are not at all favorable processes due to large endothermicities. For example, the reactions involving the ethyl cation are

$$C_2H_5^+(^1A) + O_2(^3\Sigma) \rightarrow OOH(^2A'') + C_2H_4^+(^2B_{3u}), \quad \Delta H = 166 \text{ kJ/mol} \quad (13a)$$

and

$$C_2H_5^+(^1A) + O_2(^3\Sigma) \rightarrow OOH^+(^3A'') + C_2H_4(^1A_g), \quad \Delta H = 248 \text{ kJ/mol} \quad (13b)$$

Therefore, no appreciable O_2 oxidation chemistry can be foreseen at 300 K for these species because our quantum chemical calculations predict that the approach of the triplet oxygen molecule toward the hydrocarbon cation is strongly repulsive and that the singlet/triplet crossing is not likely to be an important factor at thermal energy. This theoretical picture is consistent with the present experimental observations, which places an upper bound to the reactivity of O_2 with these hydrocarbon ions at $<5 \times 10^{-13}$ cm^3 s^{-1}. Scott et al.[7] observed that $C_2H_5^+$ also did not react with triplet atomic oxygen, even though the product channel $HCO^+ + CH_4$ is exothermic by 399 kJ/mol. These authors suggested that the barriers on the potential energy surface are too high for the extensive rearrangement required. Ozone, on the other hand, is able to produce these products in its reaction with $C_2H_5^+$, where this channel is exothermic by 294 kJ/mol (Table 1).

Ozone is a singlet in its ground state, and ab initio calculations at the B3LYP/6-31G(d) level of theory indicate that reactant complexes can be formed, decreasing in stability with the size

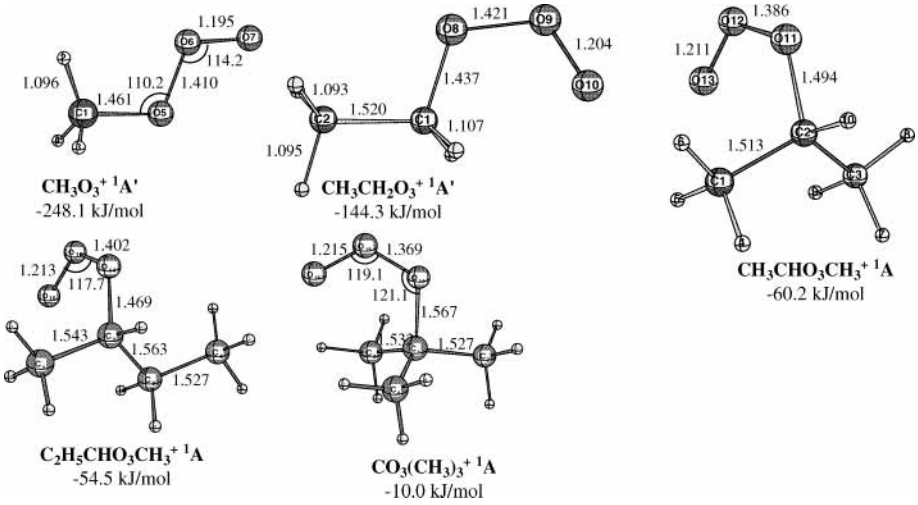

Figure 5. Initial reactant complexes for alkyl cations with ozone. Geometries were optimized at the B3LYP/6-31G(d) level of theory, bond distances are in Å, and bond angles are in degrees. Interaction energies are in kJ mol^{-1} with respect to isolated alkyl cations and ground-state ozone.

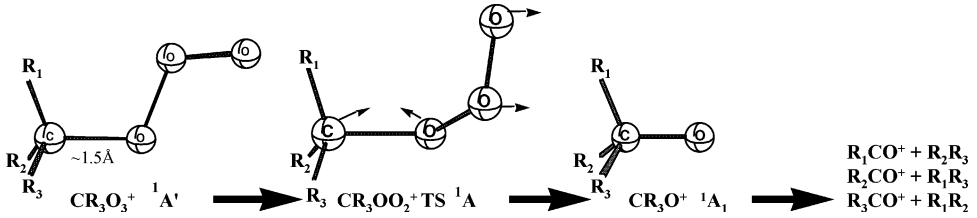

Figure 6. Proposed reaction pathway for O-atom-transfer reaction from ozone to alkyl ions. The groups labeled R_1 to R_3 (R = H, CH_3, C_2H_3) connote the species surrounding the carbon atom undergoing nucleophilic attack by ozone. After nucleophilic addition of O_3, rearrangement to a transition-state structure enabling O_2 loss follows, yielding an ionized alkyl oxide. From this structure, rearrangement can occur, leading to the product combinations listed.

of the alkyl chains attached to the cationic carbon atom. The complexes are

$$CH_3^+(^1A_{1g}) + O_3(^1A_1) \rightarrow [CH_3O_3]^+*(^1A'), \quad \Delta H = -248 \text{ kJ/mol} \quad (14a)$$

$$C_2H_5^+(1A_1) + O_3(1A_1) \rightarrow [CH_3CH_2O_3]^+(^1A'), \quad \Delta H = -144 \text{ kJ/mol} \quad (14b)$$

$$s\text{-}C_3H_7^+(^1A) + O_3(^1A_1) \rightarrow [CH_3CHO_3CH_3]^+*(^1A), \quad \Delta H = -60 \text{ kJ/mol} \quad (14c)$$

$$s\text{-}C_4H_9^+(^1A) + O_3(^1A_1) \rightarrow [CH_3CHO_3C_2H_5]^+*(^1A), \quad \Delta H = -55 \text{ kJ/mol} \quad (14d)$$

$$t\text{-}C_4H_9^+(^1A) + O_3(^1A_1) \rightarrow [CO_3(CH_3)_3]^+*(^1A), \quad \Delta H = -10 \text{ kJ/mol} \quad (14e)$$

All of these systems form a complex with a C−O distance of about 1.5 Å with no activation energy required (see Figure 5). From these complexes, rearrangement can occur, leading to several different spin-conserving products. In addition, the large exothermicity of the available reaction channels permits breaking of C−H/C−C bonds, favoring the production of smaller fragments, consistent with the experimental observations. These complexes are characterized by weak O_3−β-hydrogen interactions; α-hydrogens are not in the position to interact with the terminal oxygen atom in the initial complexes. The presence of α-hydrogens is therefore not a factor in the relative stabilities of these complexes. Drastic energetic destabilization of these initial complexes occurs when additional alkyl groups are added to the cationic carbon atom, leaving the *tert*-butyl cation/ozone complex with only a small binding energy of 10 kJ/mol.

A major product for all of the primary and secondary alkyl cations is HCO^+. The reaction pathway for this product channel could be traced computationally for the methyl cation. In the case of CH_3^+, a straightforward mechanism evolved involving nucleophilic addition of ozone to CH_3^+, early O−O_2 cleavage in the transition state with a low barrier of only 50 kJ/mol, and subsequent hydrogen elimination to yield the highly exothermic products $HCO^+ + H_2 + O_2$. The calculations indicate that H_2O_2 is not formed in this channel and that the ethyl, *sec*-propyl, and *sec*-butyl cations proceed via a similar mechanism, as illustrated in Figure 6. For $C_2H_5^+$, HCO^+ and $C_2H_3O^+$ are produced from the elimination of CH_4 and H_2, respectively, from the $[OCH_2CH_3]^+$* intermediate. Similarly, HCO^+ and $C_2H_3O^+$ are produced from the elimination of C_2H_6 and CH_4, respectively, from the $[OCH(CH_3)CH_3]^+$* intermediate. On the basis of the same mechanism, the $[OC(CH_3)_2CH_3]^+$* intermediate produced in the reaction of s-$C_4H_9^+$ is expected to produce HCO^+, $C_2H_3O^+$, and $C_3H_5O^+$ with the elimination of C_3H_8, C_2H_6 and CH_4, respectively. This mechanism is in qualitative agreement with the branching fractions observed in these reactions, as shown in Table 1, although only a barely detectable amount of $C_3H_5O^+$ reaction product is observed in the *sec*-butyl cation reaction with ozone, perhaps due to steric constraints. This mechanism is similar to that proposed by Mendes et al.[11] on the basis of their ab initio calculations of O-atom-transfer reactions of ozone with radical cations of pyridines, alkyl halides, and halogen cations.

A possible explanation for the apparent lack of reactivity of t-$C_4H_9^+$ and t-$C_5H_{11}^+$ is that the initial complex with ozone is not formed. The calculations find that the stability of the complex decreases from 248 to 10 kJ/mol on going from CH_3^+ to t-$C_4H_9^+$. Therefore, it seems likely that the lack of reactivity of the alkyl ions involving a tertiary carbocation may be attributed to a greatly reduced O_3 binding energy.

V. Summary

Numerous alkyl cations and HCO^+ reacting with O_2 and O_3 were studied at 300 K in a selected-ion flow tube coupled to a novel ozone source. The HCO^+ cation exhibits no reactivity with O_2, but the reaction of HCO^+ with O_3 proceeds at the collision rate via proton transfer to produce HO_3^+. None of the alkyl carbocations studied showed any measurable bimolecular reactivity, $k < 5 \times 10^{-13}$ cm^3 s^{-1}, with O_2, despite the availability of reaction channels with exothermicities of several hundred kilojoules per mole. The ab initio calculations indicate that the O_2 reaction systems form weak complexes with large C−O bond distances on the lowest energy triplet potential energy surface which are repulsive at smaller distances. Access to the singlet surface is required for bond formation; however, this surface is not accessible at thermal energies.

For reactions with O_3, the total reaction rate constants for the alkyl carbocations decrease dramatically as the order of the reactant carbocation increases, as shown in Figure 2 and listed in Table 1. This finding is consistent with ab initio calculations which show that the initial alkyl cation/ozone complexes are largely destabilized when alkyl groups are added to the cationic center. The primary carbocations CH_3^+ and $C_2H_5^+$ react at 100% and 46% of the collision rate given by the Su−Chesnavich equation, respectively. The secondary s-$C_3H_7^+$ and s-$C_4H_9^+$ carbocations reacted with O_3 at 19% and 7% of the collision rate, respectively. The tertiary carbocations t-$C_4H_9^+$ and t-$C_5H_{11}^+$ were found to be unreactive with O_3, $k < 5 \times 10^{-12}$ cm^3 s^{-1}, which is the detection limit of our apparatus using this ozone source. A straightforward mechanism was discussed involving initial complex formation involving the primary or secondary alkyl cation with O_3, followed by early O−O_2 cleavage in the transition state, and finally hydrogen and alkane elimination to yield the highly exothermic products listed in Table 1. An explanation for the lack of reactivity of t-$C_4H_9^+$ and t-$C_5H_{11}^+$ is that the initial complex with ozone is not formed because of a much reduced O_3 binding energy. Details of theoretical studies of the potential energy surfaces of the present systems will be published separately.

The only other positive organic ion reactions with ozone previously studied used a pentaquadrupole mass spectrometer at nonthermal (ca. 1 eV) collision energies, and thermal rate constants were not reported as done here.[11] In addition, alkyl ions were not part of that study. Therefore, the values reported in Table 1 represent the most self-consistent and complete set of reaction rate and branching fraction data reported to date and, on the basis of the above considerations, are recommended for use in modeling applications requiring thermal rate data near 300 K.

Acknowledgment. We thank John Williamson and Paul Mundis for technical support and Jane Van Doren for helpful comments regarding the manuscript. The experimental work at AFRL was supported by AFOSR (LRIR 02VS02COR), and the theoretical work at Emory was supported in part by AFOSR Grant F49620-01-10183. A.J.M. was supported through Visidyne contract no. F19628-99-C-0069.

References and Notes

(1) Fehsenfeld, F. C. *Astrophys. J.* **1976**, *209*, 638.
(2) Bohme, D. K.; Mackay, G. I.; Schiff, H. I. *J. Chem. Phys.* **1980**, *73*, 4976.
(3) Viggiano, A. A.; Howorka, F.; Albritton, D. L.; Fehsenfeld, F. C.; Adams, N. G.; Smith, D. *Astrophys. J.* **1980**, *236*, 492.
(4) Viggiano, A. A.; Morris, R. A.; Paulson, J. F.; Ferguson, E. E. *Chem. Phys. Lett.* **1988**, *148*, 296.
(5) Le Page, V.; Keheyan, Y.; Snow, T. P.; Bierbaum, V. M. *J. Am. Chem. Soc.* **1999**, *121*, 9435.
(6) Le Page, V.; Keheyan, Y.; Snow, T. P.; Bierbaum, V. M. *Int J. Mass Spectrom.* **1999**, *185/186/187*, 949.
(7) Scott, G. B. I.; Milligan, D. B.; Fairley, D. A.; Freeman, C. G.; McEwan, M. J. *J. Chem. Phys* **2000**, *112*, 4959.
(8) Maurice, L. Q.; Edwards, T.; Griffiths, J. Liquid Hydrocarbon Fuels for Hypersonic Propulsion. *Scramjet Propulsion*; AIAA Progress in Astronautics and Aeronautics Series 189; American Institute of Aeronautics and Astronautics: Reston, VA, 2000; p 757.
(9) Lawton, J.; Weinberg, F. J. *Electrical Aspects of Combustion*; Clarendon Press: Oxford, 1969.
(10) Ikezoe, Y.; Matsuoka, S.; Takebe, M.; Viggiano, A. A. *Gas-Phase Ion−Molecule Reaction Rate Constants Through 1986*; Maruzen Co., Ltd.: Tokyo, 1987.
(11) Mendes, M. A.; Moraes, L. A. B.; Sparrapan, R.; Eberlin, M. N.; Kostiainen, R.; Kotiaho, T. *J. Am. Chem. Soc.* **1998**, *120*, 7869.
(12) Becke, A. D. *J. Chem. Phys.* **1993**, *98*, 5648.
(13) Lee, C.; Yang, W.; Parr, R. G. *Phys. Rev. B* **1988**, *38*, 785.
(14) Becke, A. D. *Phys. Rev. A* **1988**, *38*, 3098.
(15) Hariharan, P. C.; Pople, J. A. *Theor. Chim. Acta* **1973**, *28*, 213.
(16) Viggiano, A. A.; Morris, R. A.; Dale, F.; Paulson, J. F.; Giles, K.; Smith, D.; Su, T. *J. Chem. Phys.* **1990**, *93*, 1149.
(17) Viggiano, A. A.; Morris, R. A. *J. Phys. Chem.* **1996**, *100*, 19227.
(18) Williams, S.; Campos, M. F.; Midey, A. J.; Arnold, S. T.; Morris, R. A.; Viggiano, A. A. *J. Phys. Chem. A* **2002**, *106*, 997.
(19) Ferguson, E. E.; Fehsenfeld, F. C.; Schmeltekopf, A. L. Flowing afterglow measurements of ion−neutral reactions. In *Advances in Atomic and Molecular Physics*; Bates, D. R., Ed.; Academic: New York, 1969; Vol. 5; p 1.
(20) Fahey, D. W.; Bohringer, H.; Fehsenfeld, F. C.; Ferguson, E. E. *J. Chem. Phys.* **1982**, *76*, 1799.
(21) Mauersberger, K.; Barnes, J.; Hanson, D.; Morton, J. *J. Geophys. Res. Lett.* **1986**, *13*, 671.
(22) DeMore, W. B.; Sander, S. P.; Golden, D. M.; Molina, M. J.; Hampson, R. F.; Kurylo, M. J.; Howard, C. J.; Ravishankara, A. R. *Chemical Kinetics and Photochemical Data for Use in Stratospheric Modeling*; Jet Propulsion Laboratory: Pasadena, CA, 1990.
(23) Ishida, K.; Morokuma, K.; Komornicki, A. *J. Chem. Phys.* **1977**, *66*, 2153.
(24) Muller, K. *Angew Chem., Int. Ed. Engl.* **1980**, *19*, 1.
(25) Schmidt, M. W.; Gordon, M. S.; Dupuis, M. *J. Am. Chem. Soc.* **1985**, *107*, 2585.
(26) Garrett, B. C.; Redmon, M. J.; Steckler, R.; Truhlar, D. G.; Baldridge, K. K.; Bartol, D.; Schmidt, M. W.; Gordon, M. S. *J. Phys. Chem.* **1988**, *92*, 1476.
(27) Baldridge, K. K.; Gordon, M. S.; Steckler, R.; Truhlar, D. G. *J. Phys. Chem.* **1989**, *93*, 5107.
(28) Mulliken, R. S. *J. Chem. Phys.* **1955**, *23*, 1833.
(29) Mulliken, R. S. *J. Chem. Phys.* **1955**, *23*, 1841.
(30) Mulliken, R. S. *J. Chem. Phys.* **1955**, *23*, 2342.
(31) Lias, S. G.; Bartmess, J. E.; Liebman, J. F.; Holmes, J. L.; Levin, R. D.; Mallard, W. G. *J. Phys. Chem. Ref. Data* **1988**, *17* (Suppl. 1), 1.
(32) Lias, S. G.; Bartmess, J. E.; Liebman, J. F.; Holmes, J. L.; Levin, R. D.; Mallard, W. G. Ion Energetics Data. In *NIST Chemistry WebBook, NIST Standard Reference Database Number 69*; Mallard, W. G., Linstrom, P. J., Eds.; NIST: Gaithersburg, 1998 (http://webbook.nist.gov).
(33) Park, S. T.; Kim, S. K.; Kim, M. S. *J. Chem. Phys.* **2001**, *115*, 2492.
(34) Keister, J. W.; Riley, J. S.; Baer, T. *J. Am. Chem. Soc.* **1993**, *115*, 12613.
(35) Szulejko, J. E.; McMahon, T. B. *J. Am. Chem. Soc.* **1993**, *115*, 7839.
(36) Smith, B. J.; Radom, L. *J. Am. Chem. Soc.* **1993**, *115*, 4885.
(37) Shold, D. M.; P., A. *J. Am. Chem. Soc.* **1978**, *100*, 7915.
(38) Scott, G. B. I.; Fairley, D. A.; Milligan, D. B.; Freeman, C. G.; McEwan, M. J. *J. Phys. Chem. A* **1999**, *103*, 7470.
(39) Mielke, Z.; Andrews, L. *J. Phys. Chem.* **1990**, *94*, 9.
(40) Smith, D.; Adams, N. G. *Int. J. Mass. Spectrosc. Ion Phys.* **1977**, *23*, 123.
(41) Adams, N. G.; Smith, D.; Lister, D. G.; Rakshit, A. B.; Tichy, M.; Twiddy, N. D. *Chem. Phys. Lett.* **1979**, *63*, 166.
(42) Koch, W.; Lin, B.; Schleyer, P. v. R. *J. Am. Chem. Soc.* **1989**, *111*, 3979.

(43) Lias, S. G.; Rebbert, R. E.; Ausloos, P. *J. Am. Chem. Soc.* **1970**, *92*, 6430.
(44) Dymerski, P. P.; Prinstein, R. M.; Bente, P. F., III; McLafferty, F. W. *J. Am. Chem. Soc.* **1976**, *98*, 6834.
(45) Attina, M.; Cacace, F.; Giacomello, P. *J. Am. Chem. Soc.* **1980**, *102*, 4768.
(46) Meot-Ner (Mautner), M.; Field, F. H. *J. Am. Chem. Soc.* **1978**, *100*, 1356.
(47) Lossing, F. P.; Holmes, J. L. *J. Am. Chem. Soc.* **1984**, *106*, 6917.
(48) Cacace, F.; Speranza, M. *Science* **1994**, *265*, 208.
(49) Fehsenfeld, F. C.; Ferguson, E. E.; Schmeltekopf, A. L. *J. Chem. Phys* **1966**, *44*, 3022.
(50) Paulson, J. F.; Mosher, R. L. *J. Chem. Phys.* **1966**, *44*, 3025.
(51) Ferguson, E. E. *Chem. Phys. Lett.* **1983**, *99*, 89.
(52) Federer, W.; Villinger, H.; Lindinger, W.; Ferguson, E. E. *Chem. Phys. Lett.* **1986**, *123*, 12.